

DESY Summer Student Programme 2009

$D^{*\pm}$ and Jets Production in Photoproduction in ep Scattering at HERA

by Mikel Berasaluce González

Universidad Autónoma de Madrid

Supervisor: Hannes Jung, Zlatka Staykova

Abstract: Inclusive production of $D^{*\pm}$ in photoproduction using the event generators CASCADE and PYTHIA is studied. Values of photon virtuality of $Q^2 < 2\text{GeV}^2$ and scattering inelasticity $0.1 < y < 0.8$ are covered. In addition, the production of jets with $D^{*\pm}$ is analysed, using the same values for photon virtuality and scattering inelasticity. Also, the difference between treating the $D^{*\pm}$ meson as a leading particle and considering inclusive jets is investigated. At the end, differential cross sections are obtained.

1 Kinematic variables

With the four-momentum of the proton $P = (E_p, \mathbf{p}_p)$, the incoming electron $k = (E_e, \mathbf{k}_e)$ and the outgoing electron $k' = (E_{e'}, \mathbf{k}_{e'})$ one can define the following variables:

$$Q^2 \equiv -q^2 \equiv -(k - k')^2$$

where q is the four-momentum of the exchanged virtual photon. Q^2 is usually called the virtuality of the photon.

The invariant mass squared (W^2) of the photon-proton system,

$$W^2 \equiv (P + q)^2$$

is equivalent to the invariant mass squared of the hadronic system in the final state.

The scattering inelasticity

$$y \equiv \frac{q \cdot P}{k \cdot P}$$

gives the fractional energy loss of the lepton in the collision.

The pseudorapidity, η , is defined

$$\eta \equiv -\ln(\tan(\frac{\theta}{2}))$$

where θ is the polar angle of the particle. Defined this way the pseudorapidity is positive in the proton direction and negative in the electron direction.

2 Photoproduction and $D^{*\pm}$ production

Photoproduction is regime corresponding to processes where the exchange photon has very small virtuality ($Q^2 \ll 1\text{GeV}^2$). In that case, the photon is near its mass-shell and can be considered quasi-real. This regime is different from the deep inelastic scattering (DIS). In DIS $Q^2 \gg 1\text{GeV}^2$ and after the collision the proton ends completely destroyed.

2.1 Heavy quark production

In ep scattering heavy quarks are dominantly produced via the boson gluon fusion (BGF) process (see figure 1).

The lightest heavy quark in the Standard Model is the charm quark, which has a mass of $m = 1.5\text{ GeV}$. It fragments to a $D^{*\pm}$ meson, which consists of a charm quark and a down quark and its mass is $m = 2.010\text{GeV}$, with a probability of 25.7%, so if an event with a $D^{*\pm}$ is found, then a charm quark-antiquark pair was produced via BGF process.

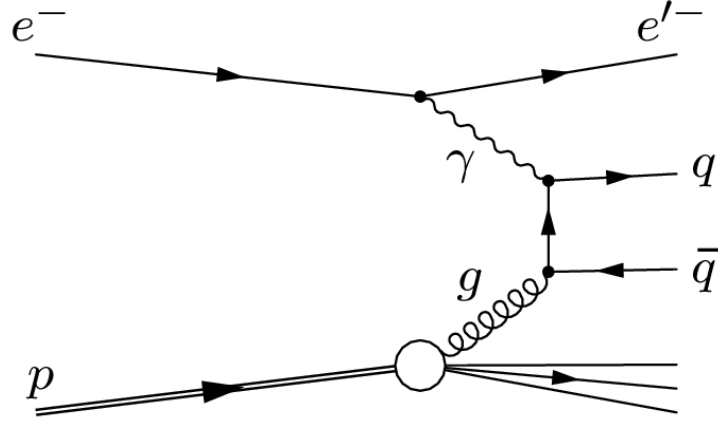


Figure 1: *Feynman diagram for BGF in deep inelastic scattering*

2.2 Hadronization: the Lund string model

In this model, the quark-antiquark pairs are bound by a colour flux tube which is called string. The force between the quark and the antiquark increases with the distance. When the string has enough energy to create a new quark-antiquark pair, it breaks. This new pair can split in another quark-antiquark pair as long as it has enough energy to create the new pair. This process continues until there is not enough energy to create a new pair. After this process ends, the quarks and the antiquarks combine into colorless hadrons.

3 Jets

A jet is a strongly collimated flow of particles, produced by the hadronization of quarks or gluons.

In this project, a cluster-type jet algorithm [1] was used to find jets. In this algorithm the final state of the collision is represented as consisting of a starting set of protojets i with momenta p_i^μ . Each protojet is characterized by its azimuthal angle ϕ_i , its pseudorapidity $\eta_i = -\ln(\tan(\frac{\theta_i}{2}))$ and its transverse energy $E_{T,i} = |\vec{p}_{T,i}|$. The algorithm depends on a parameter R , which is normally chosen to be 1. The algorithm proceeds recursively as follows:

- 1) For each protojet define

$$d_i = E_{T,i}^2$$

and for each pair of protojets define

$$d_{ij} = \min(E_{T,i}^2, E_{T,j}^2) \frac{(\eta_i - \eta_j)^2 + (\phi_i - \phi_j)^2}{R^2}.$$

- 2) Find the smallest of all the d_i and d_{ij} and label it d_{min} .
- 3) If d_{min} is a d_{ij} , merge protojets i and j into a new protojet k with:

$$E_{T,k} = E_{T,i} + E_{T,j} \quad \eta_k = \frac{E_{T,i}\eta_i + E_{T,j}\eta_j}{E_{T,k}} \quad \phi_k = \frac{E_{T,i}\phi_i + E_{T,j}\phi_j}{E_{T,k}}$$

- 4) If d_{min} is a d_i , then remove the corresponding protojet from the list of protojets and add it to the list of jets.
- 5) Go back to step 1.

This procedure continues until there are no more protojets. It produces a list of jets with successively larger $d_i = E_{T,i}^2$.

4 Motivation

In order to be able to use perturbative quantum chromo dynamics (pQCD), the virtuality of the photon has to be such that $Q^2 \gg \Lambda_{QCD}^2$, where $\Lambda_{QCD} \approx 300 \text{ MeV}$ is a threshold of the theory, because if the expansion is performed when $Q^2 \approx \Lambda_{QCD}^2$ the expansion diverges. On the other hand, the dependence of the total cross section as a function of Q is $\sigma \sim \frac{1}{Q^4}$, which means that the total ep cross section is dominated by photoproduction. In order to be able to use pQCD in the photoproduction regime, one has to use another hard scale to perform expansions; a convenient scale is m_c , because $m_c \gg \Lambda_{QCD}$.

The reason to search for $D^{*\pm}$ mesons is that they are produced by the fragmentation of a charm quark, with a probability of 27.5%. So if a $D^{*\pm}$ meson is found in an event, it means that a charm quark-antiquark pair was produced. And this pair is mainly produced via the BGF process, which involves a gluon from the proton. So investigating these events with charm quark production, one can get information about the gluons inside the proton.

5 Parton Evolution Models

5.1 DGLAP

In this DGLAP¹ model [2] the parton densities depend on Q^2 . In this model, the emitted partons are strongly ordered in the transverse momentum squared: $k_{T,i-1} \ll k_{T,i}$. All parton transverse momenta are limited from below by a fixed value Q_0^2 at which the evolution starts, and from above by the virtuality of the photon, Q^2 , such that $Q_0^2 > Q^2$.

5.2 CCFM

In this CCFM² model [3], the gluon ladder is ordered in the quantity $q = \frac{p_T}{1-z}$ where p_T is the transverse momentum of the emitted parton and z the fraction of the parent momentum carried by the emitted parton. Also ordering in emission angle is required, since $p_T = q^0 \sin \theta$: $\theta_{i+1} > \theta_i$.

¹Dokshitzer, Gribov, Lipatov, Altarelli and Parisi

²Catani, Ciafaloni, Fiorani and Marchesini

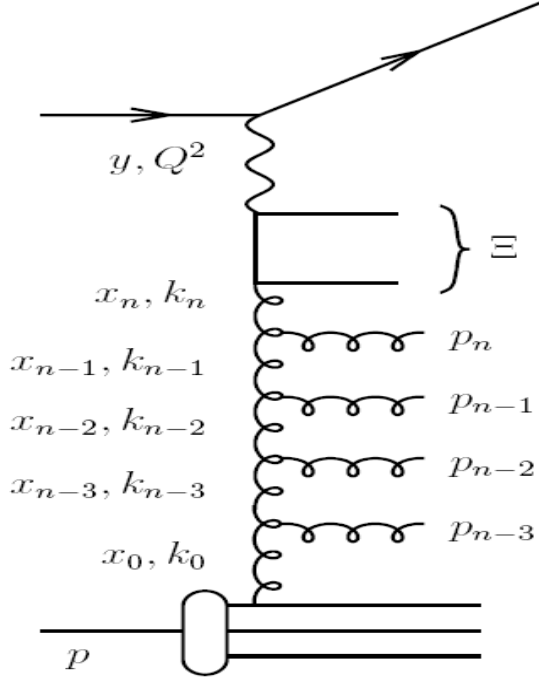


Figure 2: *Diagram for higher order processes*

6 Tools used

6.1 Monte Carlo Event Generators

6.1.1 CASCADE

CASCADE [3] is a Monte Carlo event generator that uses the CCFM evolution equation to determine the probability for a parton to branch. The matrix elements depend on k_{\perp} . For the hadronization, the Lund string model is used.

6.1.2 PYTHIA

PYTHIA [4] is a Monte Carlo event generator that uses the DGLAP parton evolution model. It also uses the Lund string model for hadronization. In this project, two different settings for this generator were used.

PYTHIA inclusive mode, where all the possible QCD processes are considered.

The second one is the direct charm production one, where always a charm quark-antiquark pair is produced.

6.2 HZTOOL

For the analysis of the events hztools were used [5].

7 HERA

The Hadron Electro Ring Accelerator (HERA) is a electron-proton collider built in Hamburg. The tunnel is 6.3 km long and it runs 10 to 25 meters underground. It began operation on November 8, 1992, and it was closed down on June 30, 2007. The electrons were accelerated to energies of 27.5GeV and the protons to energies of 920GeV , which gives a center of mass energy of 318GeV . The values of the electron and proton beam energies in the Monte Carlo generators were set to 27.5GeV and 920GeV respectively in order to simulate a collision in the HERA ep.

8 Event selection and analysis

Kinematic variable cuts of $Q^2 < 2\text{GeV}^2$ and $0.1 < y < 0.8$ were defined in order to select photoproduction. When a $D^{*\pm}$ meson is found, cuts on the $D^{*\pm}$ meson transverse momentum of $p_T(D^{*\pm}) > 1.8\text{GeV}$ and on the $D^{*\pm}$ meson pseudorapidity of $|\eta| < 1.5$, both of them measured in the laboratory frame, are imposed. Afterwards, the $D^{*\pm}$ meson is set to be stable, and all its decay products are set to be unstable so that the $D^{*\pm}$ meson can be treated as a leading particle and reconstructed in a jet quantities.

To find the jets, a k_T cluster in E recombination scheme (massive mode) algorithm (corresponding to algorithm number 9 of the hztool routine HZJTFIND) was used. It was demanded that two or more jets were produced. In the events with two or more jets, the two jets with highest transverse momentum were selected, as long as both of them fulfilled the requirements for transverse momentum $p_T(jet) > 3.0\text{GeV}$ and pseudorapidity $|\eta(jet)| < 1.5$. After the $D^{*\pm}$ meson was set to stable, the selected jets were the one containing the $D^{*\pm}$ meson and the jet with highest transverse momentum which did not contain the $D^{*\pm}$ meson. For the $D^{*\pm}$ meson jet, the transverse momentum and pseudorapidity requirements were $p_T(jet) > 3.0\text{GeV}$ and $|\eta(jet)| < 1.5$ respectively. For the other jet, the transverse momentum requirement was also $p_T(jet) > 3.0\text{GeV}$, but the pseudorapidity was considered in two different cases: $|\eta(jet)| < 1.5$ and $-1.5 < \eta(jet) < 2.9$.

In addition to differential cross section calculations of $p_t(D^{*\pm})$, $\eta(D^{*\pm})$, W , $p_t(jet)$ and $\eta(jet)$, plots were made of the invariant mass of the jets,

$$M_{jj}^{had} = \sqrt{|p(jet1) + p(jet2)|^2}$$

and its deviation from the invariant mass at partonic level, M_{jj}^{part}

$$\text{res} = \frac{M_{jj}^{part} - M_{jj}^{had}}{M_{jj}^{part}};$$

the difference in η

$$\Delta\eta = \eta(jet1) - \eta(jet2),$$

and the difference in the azimuthal angle ϕ

$$\Delta\phi = |\phi(jet1) - \phi(jet2)|.$$

To obtain the invariant mass at partonic level, two different expressions were used:

$$M_{jj}^{part} = \sqrt{|p_c + p_{\bar{c}}|^2}$$

where p_c is the momentum of the charm quark, and $p_{\bar{c}}$ the momentum of the charm antiquark; and

$$M_{jj}^{part} = \sqrt{\frac{p_{T,c}^2 + m_c^2}{z_c(1-z_c)}}$$

$$\text{where } z_c = \frac{E_c - p_{c,z}}{2E_{beam}y}.$$

Also, since the algorithm used to find jets is in massive mode, the jets were made massless before calculating M_{jj}^{had} , that way better resolutions were obtained when plotting the deviation from M_{jj}^{part} .

9 Results

9.1 $D^{*\pm}$ meson production

Differential cross sections as a function of the $D^{*\pm}$ meson transverse momentum and pseudorapidity are shown in figures 4 to 7. The total cross sections obtained integrating the histograms are:

- 1) Inclusive $D^{*\pm}$ meson
 - a) Total cross section obtained integrating $\frac{d\sigma}{dp_T}$
 - i) CASCADE: 26.3212 nb
 - i) PYTHIA inclusive mode: 29.3836 nb
 - i) PYTHIA direct mode: 19.8147 nb
 - b) Total cross section obtained integrating $\frac{d\sigma}{d\eta}$
 - i) CASCADE: 53.9983 nb
 - i) PYTHIA inclusive mode: 59.7379 nb
 - i) PYTHIA direct mode: 40.4853 nb
- 2) $D^{*\pm}$ meson after changing it to stable and selecting the $D^{*\pm}$ jet and the highest transverse momentum jet without the $D^{*\pm}$ meson, both with $p_T(jet) > 3.0 \text{ GeV}$ and $|\eta(jet)| < 1.5$
 - a) Total cross section obtained integrating $\frac{d\sigma}{dp_T}$
 - i) CASCADE: 13.0136 nb
 - i) PYTHIA inclusive mode: 13.8757 nb
 - i) PYTHIA direct mode: 10.804 nb
 - b) Total cross section obtained integrating $\frac{d\sigma}{d\eta}$
 - i) CASCADE: 15.3793 nb
 - i) PYTHIA inclusive mode: 16.329 nb
 - i) PYTHIA direct mode: 12.9604 nb

The results obtained for CASCADE and for PYTHIA inclusive mode are quite similar, while the results for PYTHIA direct mode are much lower than the others. This is because in the direct mode only point-like photons interacting directly with the quarks are considered, while in the other cases more processes are considered, like the one with a resolved photon.

9.2 Invariant mass of jets

The differential cross sections as a function of the invariant mass of the jets, M_{jj}^{had} , are shown in figures 8 to 10. Changing the $D^{*\pm}$ meson to stable and all its daughters to unstable, or selecting the $D^{*\pm}$ meson jet and the jet with highest transverse momentum instead of selecting the two jets with highest transverse momentum without looking for the $D^{*\pm}$ doesn't produce any real difference in the differential cross sections. In all three cases, both CASCADE and PYTHIA inclusive mode give almost the same differential cross section.

The deviation of the invariant mass of the jets, M_{jj}^{had} , from the invariant mass at partonic level, M_{jj}^{part} is shown in figures 11 to 16. The mean value and the RMS for each histogram are as follow:

1) Before changing the $D^{*\pm}$ to stable.

- a) Using $M_{jj}^{part} = \sqrt{|p_c + p_{\bar{c}}|^2}$
 - i) CASCADE mean: -0.04026
 - ii) CASCADE RMS: 0.4361
 - iii) PYTHIA inclusive mode mean: 0.06147
 - iv) PYTHIA inclusive mode RMS: 0.3703
 - v) PYTHIA direct mode mean: 0.0133
 - vi) PYTHIA direct mode RMS: 0.2835
- b) Using $M_{jj}^{part} = \sqrt{\frac{p_{T,c}^2 + m_c^2}{z_c(1-z_c)}}$
 - i) CASCADE mean: 0.5272
 - ii) CASCADE RMS: 0.4159
 - iii) PYTHIA inclusive mode mean: 0.1259
 - iv) PYTHIA inclusive mode RMS: 0.3263
 - v) PYTHIA direct mode mean: 0.1177
 - vi) PYTHIA direct mode RMS: 0.3075

2) After changing the $D^{*\pm}$ to stable and selecting the two highest transverse momentum jets.

- a) Using $M_{jj}^{part} = \sqrt{|p_c + p_{\bar{c}}|^2}$
 - i) CASCADE mean: -0.07681
 - ii) CASCADE RMS: 0.4285
 - iii) PYTHIA inclusive mode mean: 0.008258
 - iv) PYTHIA inclusive mode RMS: 0.3786
 - v) PYTHIA direct mode mean: 0.04837
 - vi) PYTHIA direct mode RMS: 0.2967
- b) Using $M_{jj}^{part} = \sqrt{\frac{p_{T,c}^2 + m_c^2}{z_c(1-z_c)}}$
 - i) CASCADE mean: 0.01358
 - ii) CASCADE RMS: 0.4129
 - iii) PYTHIA inclusive mode mean: 0.07479
 - iv) PYTHIA inclusive mode RMS: 0.3433
 - v) PYTHIA direct mode mean: 0.06346

- vi) PYTHIA direct mode RMS: 0.3236
- 3) After changing the $D^{*\pm}$ to stable and selecting the $D^{*\pm}$ meson jet and the highest transverse momentum jet without the $D^{*\pm}$ meson.
 - a) Using $M_{jj}^{part} = \sqrt{|p_c + p_{\bar{c}}|^2}$
 - i) CASCADE mean: -0.04021
 - ii) CASCADE RMS: 0.3975
 - iii) PYTHIA inclusive mode mean: 0.02257
 - iv) PYTHIA inclusive mode RMS: 0.3739
 - v) PYTHIA direct mode mean: 0.06377
 - vi) PYTHIA direct mode RMS: 0.2878
 - b) Using $M_{jj}^{part} = \sqrt{\frac{p_{T,c}^2 + m_c^2}{z_c(1-z_c)}}$
 - i) CASCADE mean: 0.0477
 - ii) CASCADE RMS: 0.3902
 - iii) PYTHIA inclusive mode mean: 0.09262
 - iv) PYTHIA inclusive mode RMS: 0.3318
 - v) PYTHIA direct mode mean: 0.0807
 - vi) PYTHIA direct mode RMS: 0.3147

Better values for both the mean value and the RMS are usually obtained when $M_{jj}^{part} = \sqrt{|p_c + p_{\bar{c}}|^2}$ instead of $M_{jj}^{part} = \sqrt{\frac{p_{T,c}^2 + m_c^2}{z_c(1-z_c)}}$ is considered, so $M_{jj}^{part} = \sqrt{|p_c + p_{\bar{c}}|^2}$ is a better choice for the invariant mass at parton level.

9.3 Transverse momentum and pseudorapidity of jets

Differential cross sections as a function of the transverse momentum and the pseudorapidity of the $D^{*\pm}$ jet and the highest transverse momentum jet without the $D^{*\pm}$ meson are shown in figures 17 to 24. Figures 17 to 20 correspond to the cuts $p_T(jets) > 3.0 \text{ GeV}$, $|\eta(jets)| < 1.5$; and figures 21 to 24 correspond to the cuts $p_T(jets) > 3.0 \text{ GeV}$, $|\eta(D^{*\pm}jet)| < 1.5$, $-1.5 < \eta(otherjet) < 2.9$.

In both cases, the results obtained for CASCADE and PYTHIA are similar for the differential cross sections of the $D^{*\pm}$ jet and for the differential cross section as a function of the transverse momentum on the other jet. But they are completely different for the differential cross section as a function of the pseudorapidity of the other jet. This is seen better in figure 23, where graphic corresponding to CASCADE is shifted towards the forward direction, being centered between $\eta = 1.0$ and $\eta = 1.5$ while the ones corresponding to PYTHIA are centered in $\eta = 0$.

9.4 Inclusive jets and $D^{*\pm}$ meson leading jets

Differential cross sections as a function of the transverse momentum and the pseudorapidity of the two highest transverse momentum jets for the cuts $p_T(jets) > 3.0 \text{ GeV}$, $|\eta(jets)| < 1.5$ are shown in figures 25 to 32. The ones for the two highest transverse momentum jets after selecting the $D^{*\pm}$ meson are shown in figures 25 to 28. The ones for the two highest transverse momentum jets after changing the $D^{*\pm}$ meson to stable are shown in figures 29 to 32.

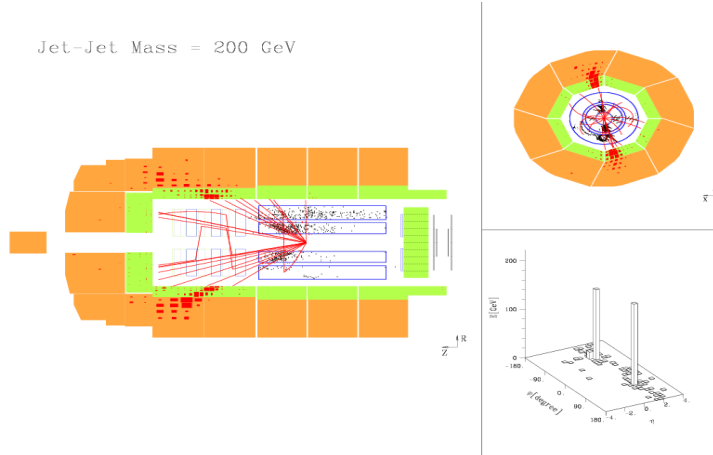


Figure 3: *2-jet photoproduction event at H1*

In both cases CASCADE and PYTHIA give similar results for the differential cross sections as a function of the transverse momentum of both jets and the pseudorapidity of the first jet, but the results are different for the pseudorapidity of the second jet. In this case, the results for CASCADE are shifted in the forward direction while the results for PYTHIA are shifted in the opposite direction.

Also is noteworthy that the results obtained considering the $D^{*\pm}$ meson as part of the jets are slightly different for the ones obtained when the particles in the jet are the decay products of the $D^{*\pm}$ meson. This might be because when reconstructing the jet, the algorithm may assign one of the decay products to a jet that it is not the correct one.

9.5 Difference of pseudorapidity, $\Delta\eta$, and azimuthal angle, $\Delta\phi$, of jets

Differential cross sections as a function of the difference of pseudorapidity and azimuthal angle of jets are shown in figures 33 to 40. Figures 33 to 36 correspond to the cuts $p_T(jets) > 3.0 \text{ GeV}$, $|\eta(jets)| < 1.5$; and figures 37 to 40 correspond to the cuts $p_T(jets) > 3.0 \text{ GeV}$, $|\eta(D^{*\pm}jet)| < 1.5$, $-1.5 < \eta(otherjet) < 2.9$.

The study of differential cross sections as a function of $\Delta\eta$ and $\Delta\phi$ is interesting because, when there is a clean event like the one shown in figure 3, where there are only two jets, which come from the hadronization of the charm quark and antiquark, it usually corresponds to $\Delta\phi \approx 180^\circ$ and $\Delta\eta \approx 0$. But there are some events with large difference in the pseudorapidity and small difference in the azimuthal angle. In those events, the selected jets are not the ones associated to the charm quark and antiquark, but the jets associated to the $D^{*\pm}$ meson, that it is associated to the charm quark or antiquark, and a jet associated to a gluon that has been emitted.

Also, when looking at the differential cross sections as a function of $\Delta\phi$ for $|\Delta\eta| > 1.0$, one can notice that, for small differences in angle, the differential cross section when we consider jets without the $D^{*\pm}$ meson with pseudorapidity $-1.5 < \eta(otherjet) < 2.9$ is higher than the one obtained when jets without the $D^{*\pm}$ meson with pseudorapidity $-1.5 < \eta(otherjet) < 1.5$ are considered. This is because when we allow the second jet to have a higher pseudorapidity, more events where the second jet is associated to a gluon are considered.

Another thing that can be observed is that when $\Delta\phi$ decreases, the differential cross sections obtained using PYTHIA decrease faster than obtained when using CASCADE.

10 Conclusion

When studying the differential cross sections as a function of variables like the transverse momentum of the jets, both CASCADE and PYTHIA give very similar results, but in other cases, like in the differential cross sections as a function of the difference in the azimuthal angle, the results are completely different, so the study of $D^{*\pm}$ meson production events is a powerful tool to compare different physical models, using the results from CASCADE and PYTHIA.

11 Acknowledgments

I would like to thank Dr. Hannes Jung and my officemate Zlatka Staykova for their supervision and support throughout this project. I would also like to thank my other officemate Axel Cholewa for his help and time when I had problems with my project.

12 References

- 1) S. D. Ellis and D. E. Soper, *Successive combination jet algorithm for hadron collisions*, Phys. Rev. **D48** (1993), 3160, hep-ph/9305266.
- 2) Zlatka Georgieva Staykova, *Charm Production with Associated jets in the Forward Direction at HERA*.
- 3) H. Jung and G. P. Salam, *Hadronic final state predictions from CCFM: The hadron level Monte Carlo generator CASCADE*, Eur. Phys. J. **C19** (2001), 351, hep-ph/0012143.
- 4) T. Sjöstrand, S. Mrenna, P. Skands, *A Brief Introduction to PYTHIA 8.1*.
- 5) J. M. Butterworth, H. Jung, E. L. Nurse, B. M. Waugh, *HZTOOL A Library for Data - Simulation Comparisons at High Energy Colliders*.

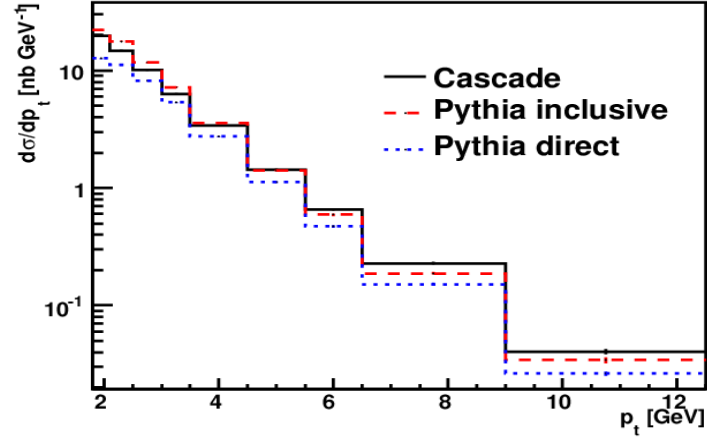


Figure 4: *Differential cross section as a function of the transversal momentum of the $D^{*\pm}$ meson after the cuts $p_T(D^{*\pm}) > 1.8 \text{ GeV}$ and $|\eta(D^{*\pm})| < 1.5$*

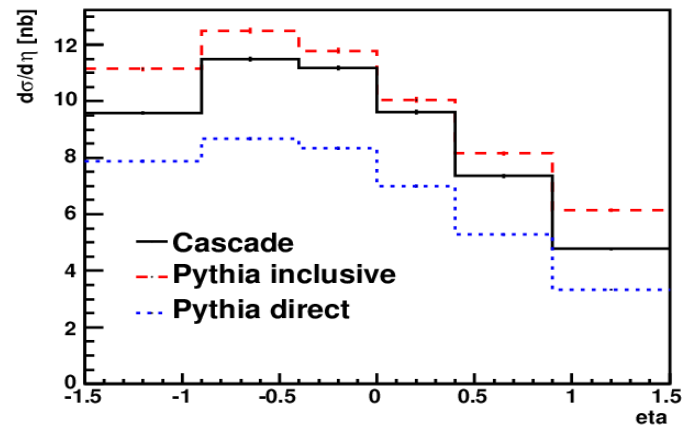


Figure 5: *Differential cross section as a function of the pseudorapidity of the $D^{*\pm}$ meson after the cuts $p_T(D^{*\pm}) > 1.8 \text{ GeV}$ and $|\eta(D^{*\pm})| < 1.5$*

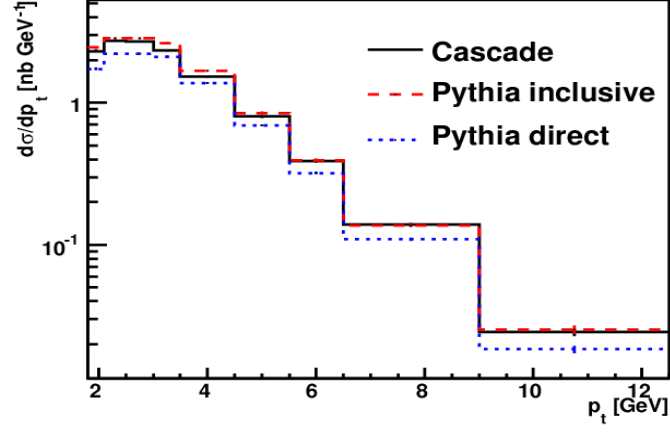


Figure 6: *Differential cross section as a function of the transversal momentum of the $D^{*\pm}$ meson for the cuts $p_T(jets) > 3.0 \text{ GeV}$, $|\eta(D^{*\pm}jet)| < 1.5$, $|\eta(otherjet)| < 1.5$*

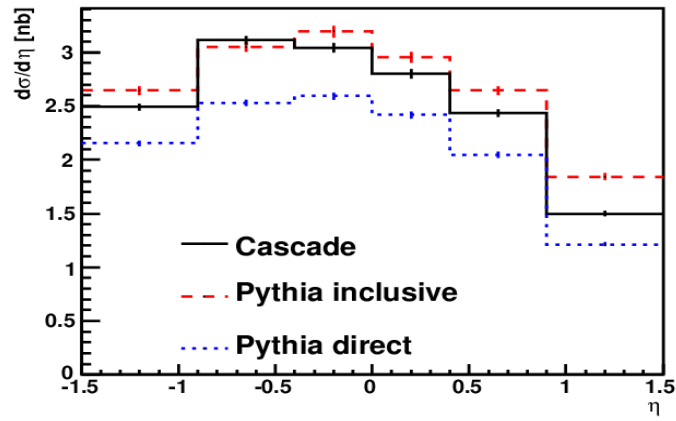


Figure 7: *Differential cross section as a function of the pseudorapidity of the $D^{*\pm}$ meson $p_T(jets) > 3.0 \text{ GeV}$, $|\eta(D^{*\pm}jet)| < 1.5$, $|\eta(otherjet)| < 1.5$*

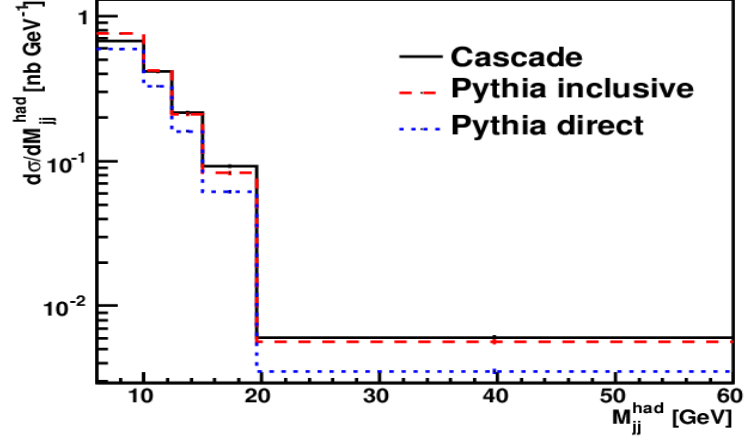


Figure 8: *Differential cross section as a function of the invariant mass of the jets for the cuts $p_T(\text{jets}) > 3.0 \text{ GeV}$, $|\eta(\text{jets})| < 1.5$, before changing the $D^{*\pm}$ to stable*

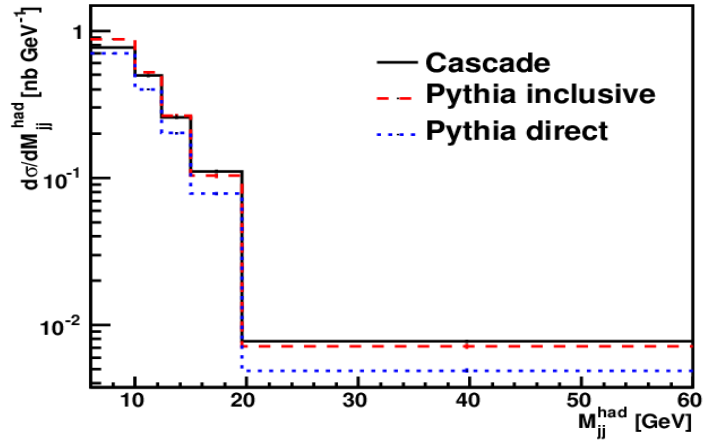


Figure 9: *Differential cross section as a function of the invariant mass of the jets for the cuts $p_T(\text{jets}) > 3.0 \text{ GeV}$, $|\eta(\text{jets})| < 1.5$, after changing the $D^{*\pm}$ to stable*

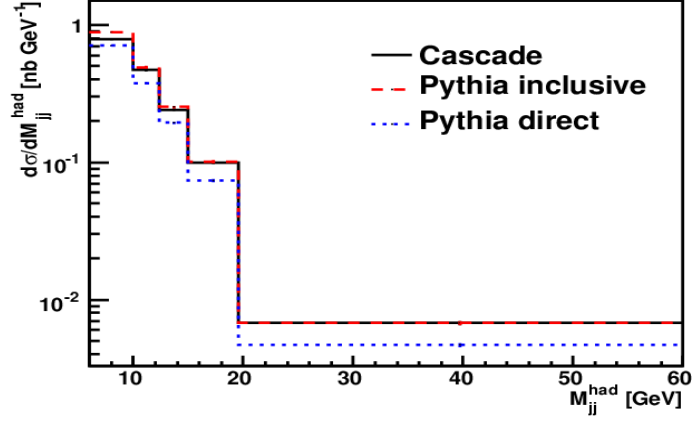


Figure 10: *Differential cross section as a function of the invariant mass of the jets for the cuts $p_T(\text{jets}) > 3.0 \text{ GeV}$, $|\eta(D^{*\pm}\text{jet})| < 1.5$, $|\eta(\text{otherjet})| < 1.5$*

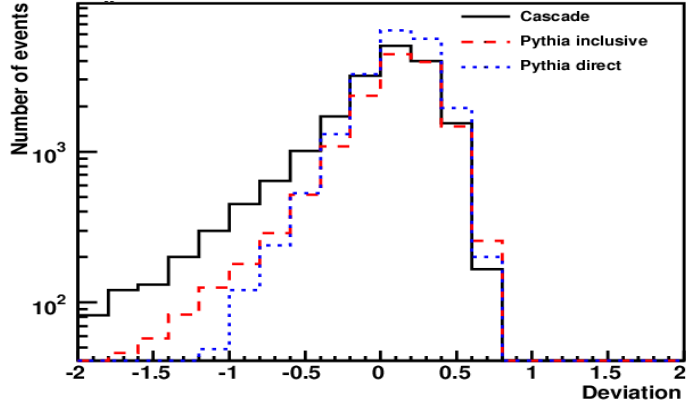


Figure 11: *Deviation of the invariant mass of the jets for the cuts $p_T(\text{jets}) > 3.0 \text{ GeV}$, $|\eta(\text{jets})| < 1.5$, before changing the $D^{*\pm}$ to stable, using $M_{jj}^{part} = \sqrt{|p_c + p_{\bar{c}}|^2}$*

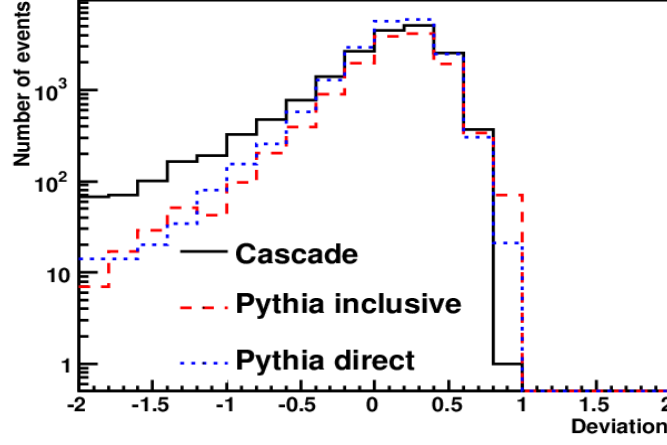


Figure 12: Deviation of the invariant mass of the jets for the cuts $p_T(\text{jets}) > 3.0 \text{ GeV}$, $|\eta(\text{jets})| < 1.5$, before changing the $D^{*\pm}$ to stable, using $M_{jj}^{part} = \sqrt{\frac{p_{T,c}^2 + m_c^2}{z_c(1-z_c)}}$

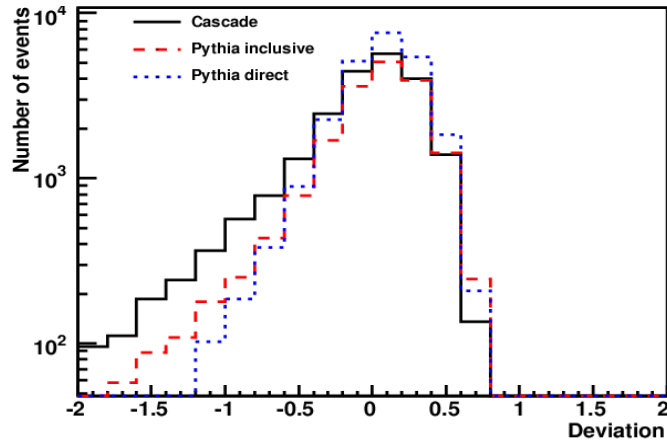


Figure 13: Deviation of the invariant mass of the jets for the cuts $p_T(\text{jets}) > 3.0 \text{ GeV}$, $|\eta(\text{jets})| < 1.5$, after changing the $D^{*\pm}$ to stable, using $M_{jj}^{part} = \sqrt{|p_c + p_{\bar{c}}|^2}$

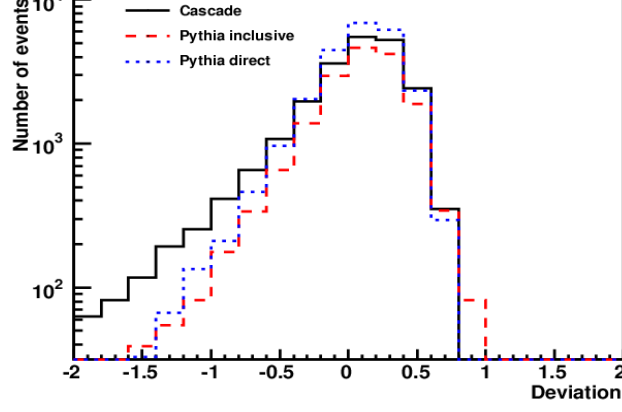


Figure 14: *Deviation of the invariant mass of the jets for the cuts $p_T(\text{jets}) > 3.0 \text{ GeV}$, $|\eta(\text{jets})| < 1.5$, after changing the $D^{*\pm}$ to stable, using $M_{jj}^{part} = \sqrt{\frac{p_{T,c}^2 + m_c^2}{z_c(1-z_c)}}$*

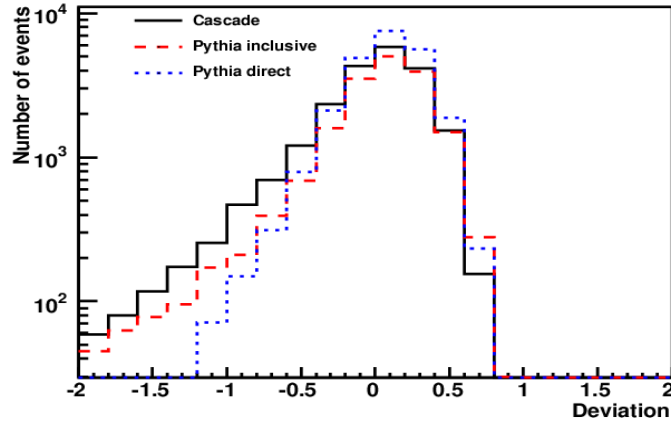


Figure 15: *Deviation of the invariant mass of the jets for the cuts $p_T(\text{jets}) > 3.0 \text{ GeV}$, $|\eta(D^{*\pm} \text{jet})| < 1.5$, $|\eta(\text{otherjet})| < 1.5$ using $M_{jj}^{part} = \sqrt{|p_c + p_{\bar{c}}|^2}$*

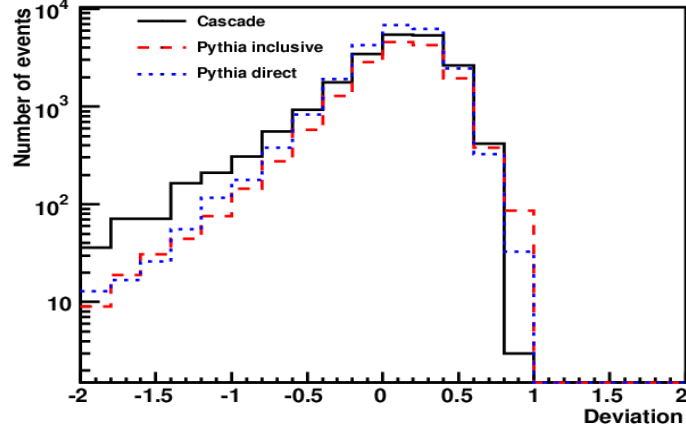


Figure 16: *Deviation of the invariant mass of the jets for the cuts $p_T(\text{jets}) > 3.0 \text{ GeV}$, $|\eta(D^{*\pm}\text{jet})| < 1.5$, $|\eta(\text{otherjet})| < 1.5$ using $M_{jj}^{\text{part}} = \sqrt{\frac{p_{T,c}^2 + m_c^2}{z_c(1-z_c)}}$*

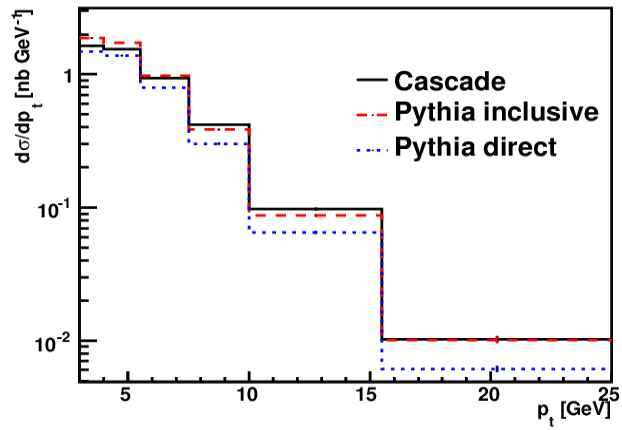


Figure 17: *Differential cross section as a function of the transverse momentum of the $D^{*\pm}$ jet for the cuts $p_T(\text{jets}) > 3.0 \text{ GeV}$, $|\eta(D^{*\pm}\text{jet})| < 1.5$, $|\eta(\text{otherjet})| < 1.5$*

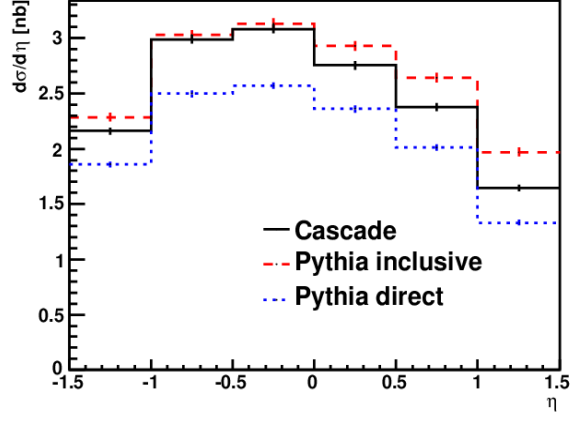


Figure 18: *Differential cross section as a function of the pseudorapidity of the $D^{*\pm}$ jet for the cuts $p_T(\text{jets}) > 3.0 \text{ GeV}$, $|\eta(D^{*\pm}\text{jet})| < 1.5$, $|\eta(\text{otherjet})| < 1.5$*

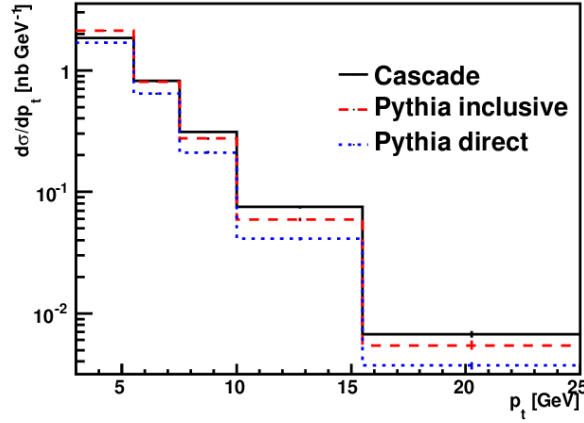


Figure 19: *Differential cross section as a function of the transverse momentum of the jet without the $D^{*\pm}$ meson for the cuts $p_T(\text{jets}) > 3.0 \text{ GeV}$, $|\eta(D^{*\pm}\text{jet})| < 1.5$, $|\eta(\text{otherjet})| < 1.5$*

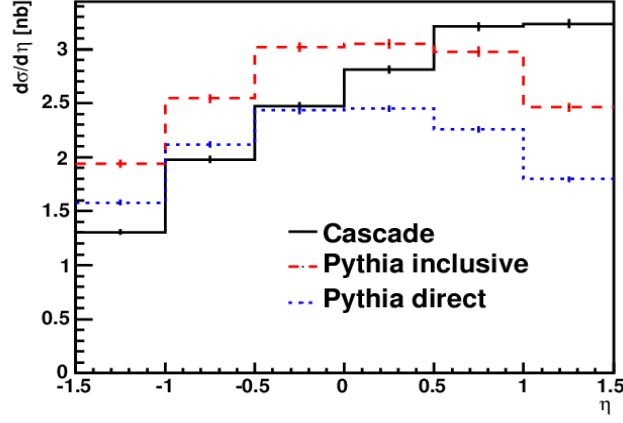


Figure 20: *Differential cross section as a function of the pseudorapidity of the jet without the $D^{*\pm}$ meson for the cuts $p_T(\text{jets}) > 3.0 \text{ GeV}$, $|\eta(D^{*\pm}\text{jet})| < 1.5$, $|\eta(\text{otherjet})| < 1.5$*

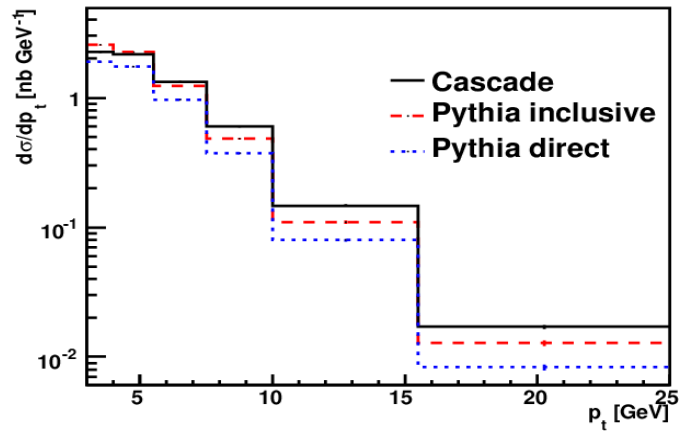


Figure 21: *Differential cross section as a function of the transverse momentum of the $D^{*\pm}$ jet for the cuts $p_T(\text{jets}) > 3.0 \text{ GeV}$, $|\eta(D^{*\pm}\text{jet})| < 1.5$, $-1.5 < \eta(\text{otherjet}) < 2.9$*

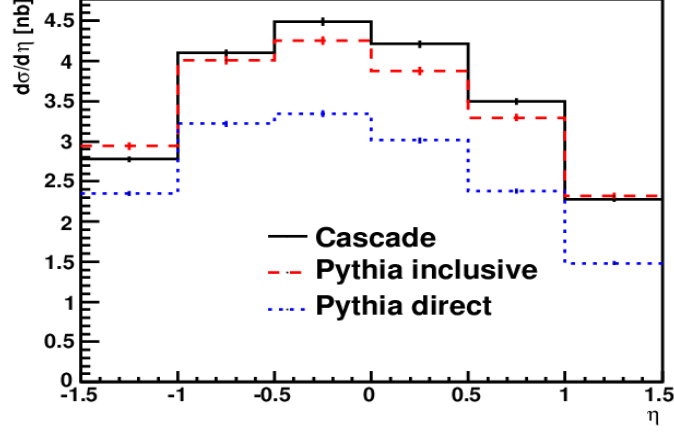


Figure 22: *Differential cross section as a function of the pseudorapidity of the $D^{*\pm}$ jet for the cuts $p_T(\text{jets}) > 3.0 \text{ GeV}$, $|\eta(D^{*\pm}\text{jet})| < 1.5$, $-1.5 < \eta(\text{otherjet}) < 2.9$*

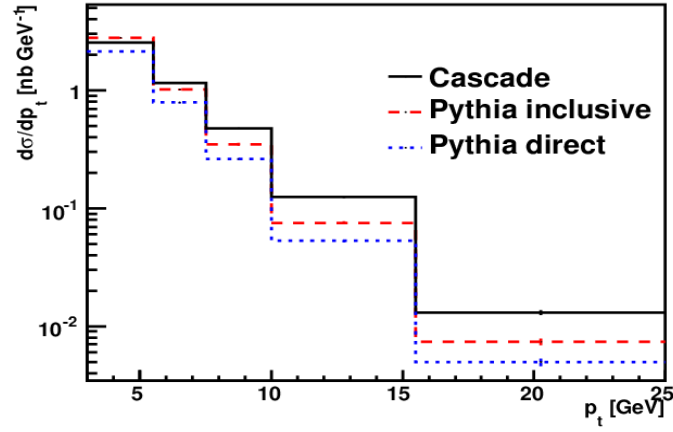


Figure 23: *Differential cross section as a function of the transverse momentum of the jet without the $D^{*\pm}$ meson for the cuts $p_T(\text{jets}) > 3.0 \text{ GeV}$, $|\eta(D^{*\pm}\text{jet})| < 1.5$, $-1.5 < \eta(\text{otherjet}) < 2.9$*

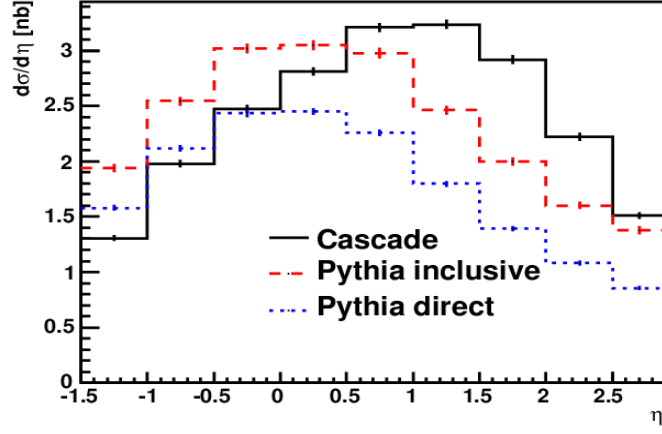


Figure 24: *Differential cross section as a function of the pseudorapidity of the jet without the $D^{*\pm}$ meson for the cuts $p_T(\text{jets}) > 3.0 \text{ GeV}$, $|\eta(D^{*\pm}\text{jet})| < 1.5$, $-1.5 < \eta(\text{other jet}) < 2.9$*

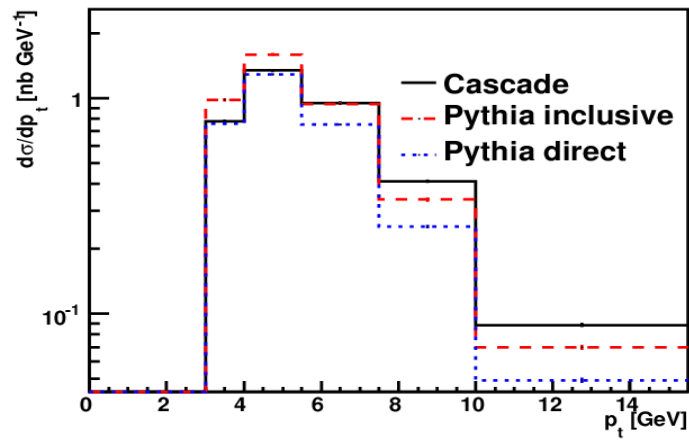


Figure 25: *Differential cross section as a function of the transverse momentum of the jet with highest transverse momentum just after selecting the $D^{*\pm}$ meson*

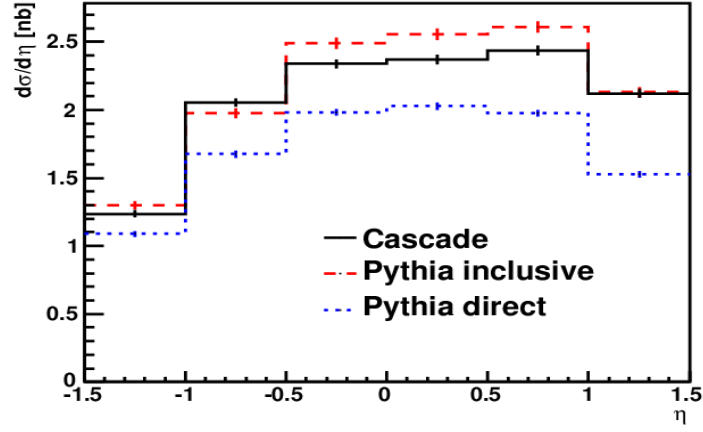


Figure 26: *Differential cross section as a function of the pseudorapidity of the jet with highest transverse momentum just after selecting the $D^{*\pm}$ meson*

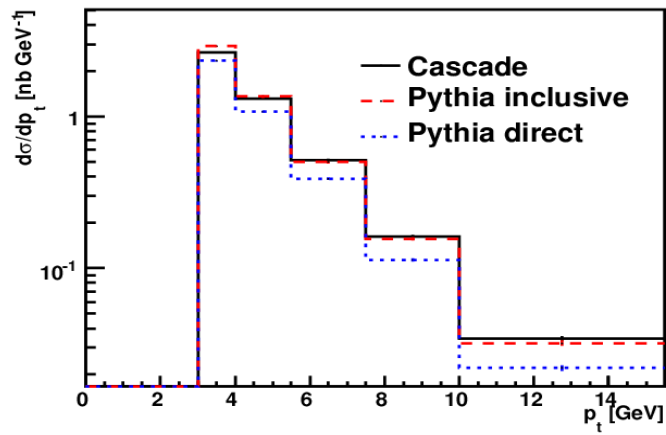


Figure 27: *Differential cross section as a function of the transverse momentum of the jet with the second highest transverse momentum just after selecting the $D^{*\pm}$ meson*

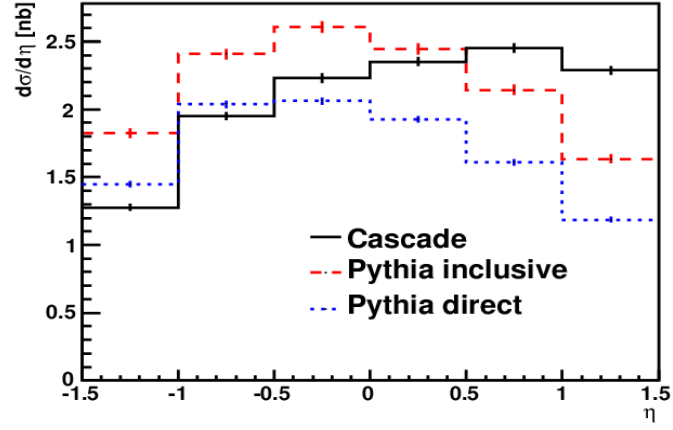


Figure 28: *Differential cross section as a function of the pseudorapidity of the jet with the second highest transverse momentum just after selecting the $D^{*\pm}$ meson*

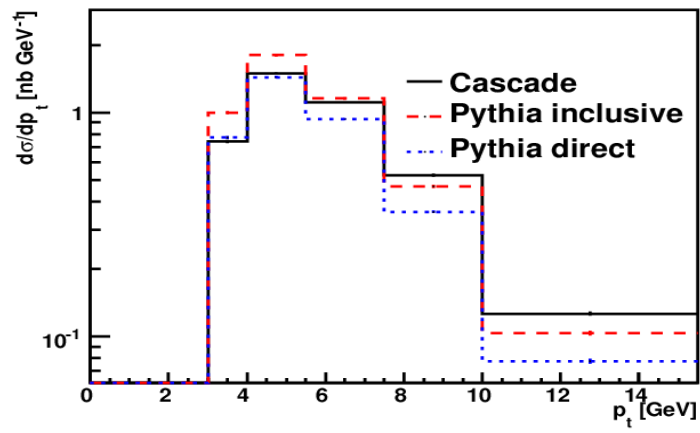


Figure 29: *Differential cross section as a function of the transverse momentum of the jet with highest transverse momentum just after changing the $D^{*\pm}$ meson to stable*

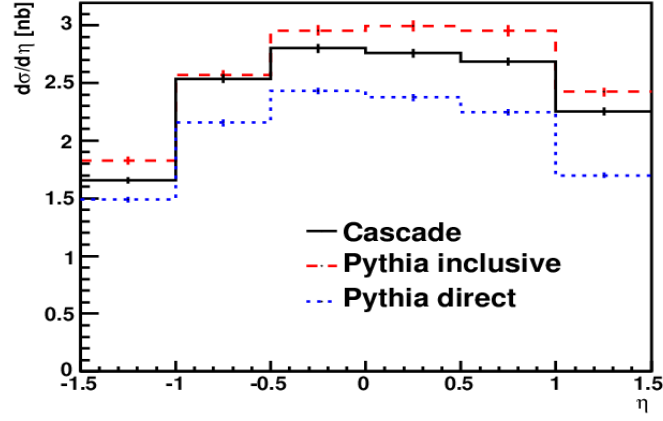


Figure 30: *Differential cross section as a function of the pseudorapidity of the jet with highest transverse momentum just after changing the $D^{*\pm}$ meson to stable*

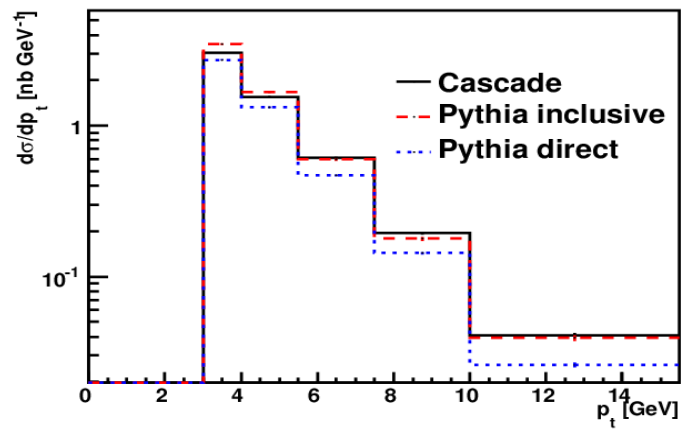


Figure 31: *Differential cross section as a function of the transverse momentum of the jet with the second highest transverse momentum just after changing the $D^{*\pm}$ meson to stable*

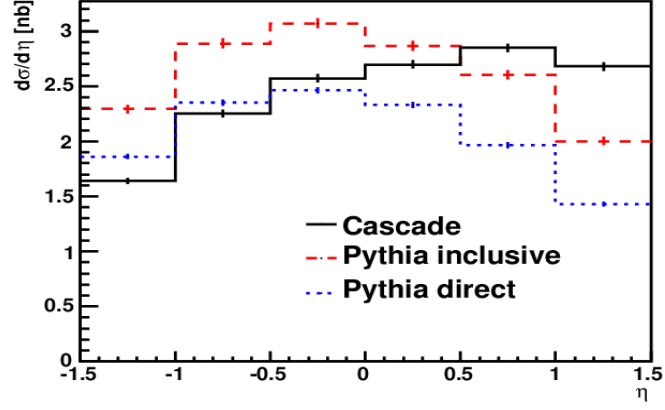


Figure 32: *Differential cross section as a function of the pseudorapidity of the jet with the second highest transverse momentum just after changing the $D^{*\pm}$ meson to stable*

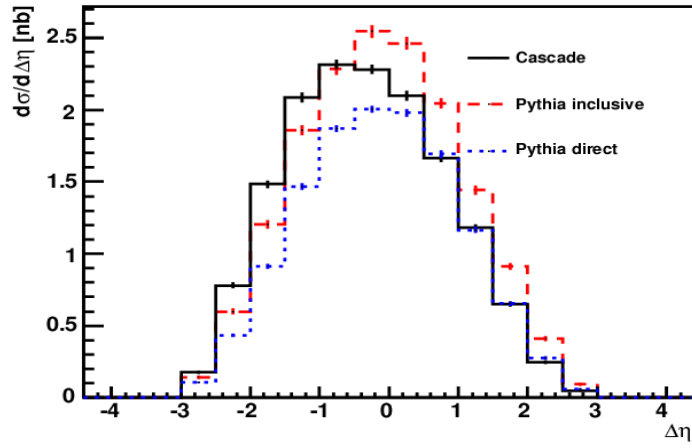


Figure 33: *Differential cross section as a function of $\Delta\phi$ of the $D^{*\pm}$ jet for the cuts $p_T(\text{jets}) > 3.0 \text{ GeV}$, $|\eta(D^{*\pm}\text{jet})| < 1.5$, $|\eta(\text{other jet})| < 1.5$, for $|\Delta\eta| < 1.0$*

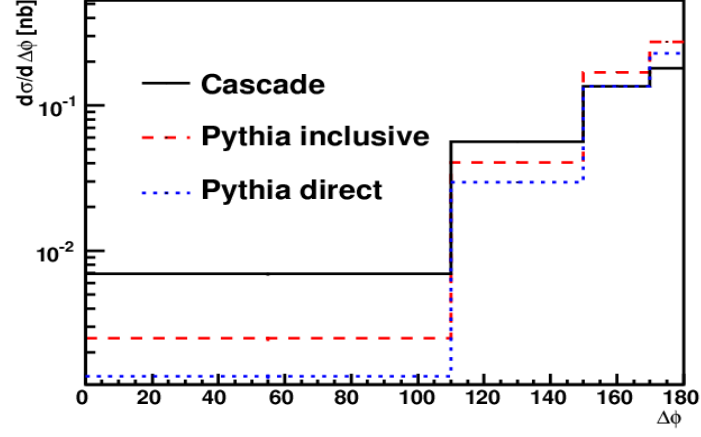


Figure 34: *Differential cross section as a function of $\Delta\phi$ of the $D^{*\pm}$ jet for the cuts $p_T(\text{jets}) > 3.0 \text{ GeV}$, $|\eta(D^{*\pm}\text{jet})| < 1.5$, $|\eta(\text{otherjet})| < 1.5$, for $|\Delta\eta| > 1.0$*

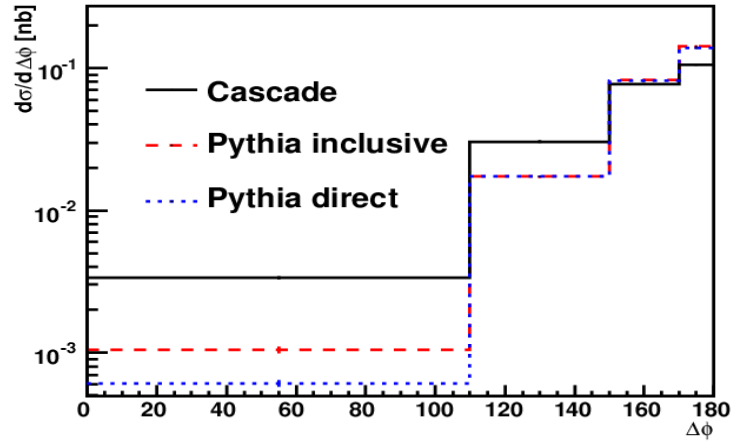


Figure 35: *Differential cross section as a function of $\Delta\phi$ of the jet without the $D^{*\pm}$ meson for the cuts $p_T(\text{jets}) > 3.0 \text{ GeV}$, $|\eta(D^{*\pm}\text{jet})| < 1.5$, $|\eta(\text{otherjet})| < 1.5$, for $|\Delta\eta| < 1.0$*

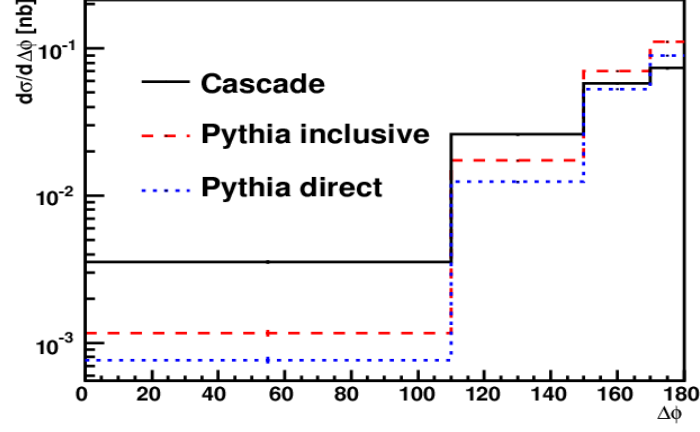


Figure 36: *Differential cross section as a function of $\Delta\phi$ of the jet without the $D^{*\pm}$ meson for the cuts $p_T(\text{jets}) > 3.0 \text{ GeV}$, $|\eta(D^{*\pm}\text{jet})| < 1.5$, $|\eta(\text{otherjet})| < 1.5$, for $|\Delta\eta| > 1.0$*

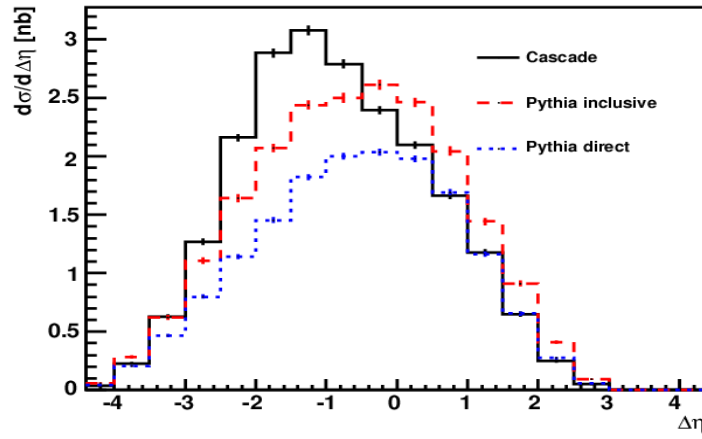


Figure 37: *Differential cross section as a function of $\Delta\eta$ of the jet without the $D^{*\pm}$ meson for the cuts $p_T(\text{jets}) > 3.0 \text{ GeV}$, $|\eta(D^{*\pm}\text{jet})| < 1.5$, $-1.5 < \eta(\text{otherjet}) < 2.9$*

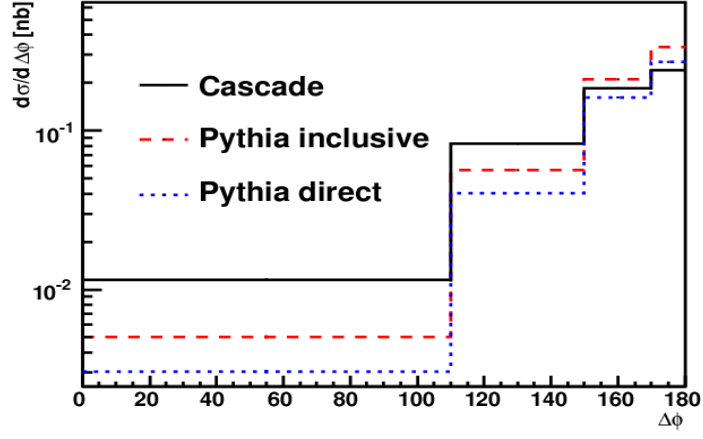


Figure 38: *Differential cross section as a function of $\Delta\phi$ of the jet without the $D^{*\pm}$ meson for the cuts $p_T(\text{jets}) > 3.0 \text{ GeV}$, $|\eta(D^{*\pm}\text{jet})| < 1.5$, $-1.5 < \eta(\text{otherjet}) < 2.9$*

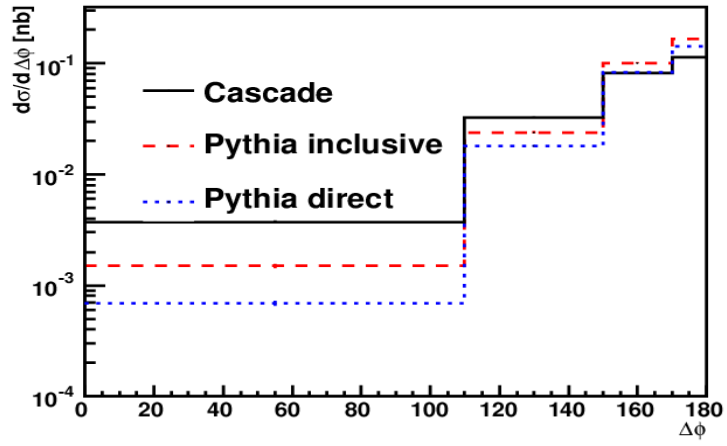


Figure 39: *Differential cross section as a function of $\Delta\phi$ of the jet without the $D^{*\pm}$ meson for the cuts $p_T(\text{jets}) > 3.0 \text{ GeV}$, $|\eta(D^{*\pm}\text{jet})| < 1.5$, $-1.5 < \eta(\text{otherjet}) < 2.9$ for $|\Delta\eta| < 1.0$*

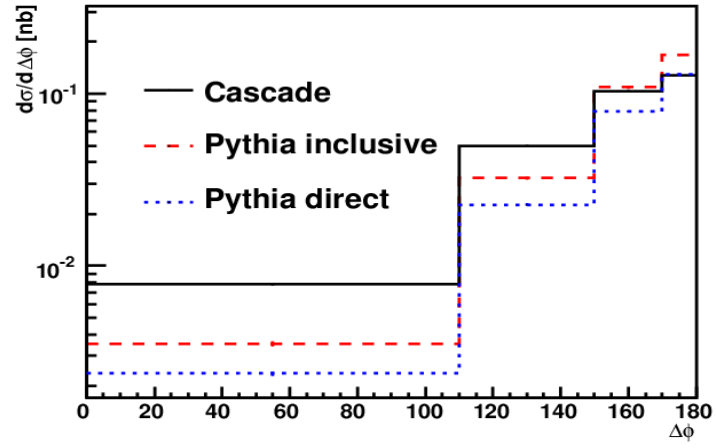


Figure 40: *Differential cross section as a function of $\Delta\phi$ of the jet without the $D^{*\pm}$ meson for the cuts $p_T(\text{jets}) > 3.0 \text{ GeV}$, $|\eta(D^{*\pm}\text{jet})| < 1.5$, $-1.5 < \eta(\text{other jet}) < 2.9$ for $|\Delta\eta| > 1.0$*